PERGAMON

International Journal of Solids and Structures 38 (2001) 9359–9381

INTERNATIONAL JOURNAL OF SOLIDS and STRUCTURES

www.elsevier.com/locate/ijsolstr

Static and dynamic characterization of regular truncated icosahedral and dodecahedral tensegrity modules

Hidenori Murakami *, Yoshitaka Nishimura

Department of Mechanical and Aerospace Engineering, University of California at San Diego, 9500 Gilman Drive, La Jolla, CA 92093-0411, USA

Received 10 December 1999

Abstract

Static and dynamic properties of a pair of dual spherical tensegrity modules invented by Buckminster Fuller are investigated. They are regular truncated icosahedral and dodecahedral tensegrity modules. The computation of the Maxwell number and the use of Calladine's relation reveal that regular truncated icosahedral and dodecahedral tensegrity modules possess 55 infinitesimal mechanism modes. A reduced equilibrium matrix is presented for the initial shape finding to economically impose the existence of a pre-stress mode. Both the initial shape and the corresponding pre-stress mode are analytically obtained by using graphs of the icosahedral group and the reduced equilibrium matrix. For both icosahedral and dodecahedral modules the maximum values of the cable tension is always less than the absolute value of bar compression. In order to classify a large number of infinitesimal mechanism modes, modal analyses are conducted. Infinitesimal mechanism modes have the stiffness due to pre-stress and are associated with lowest natural frequencies. Their natural frequencies increase proportionally to the square root of the amplitude of pre-stress. It is found that there are only 15 distinct natural frequencies associated with the infinitesimal mechanism modes. © 2001 Elsevier Science Ltd. All rights reserved.

Keywords: Icosahedral tensegrity; Dodecahedral tensegrity; Initial shape finding; Modal analysis

1. Introduction

Tensegrity structures are a class of truss structures consisting of a continuous set of tension members (cables) and a discrete set of compression members (bars). Kenneth Snelson originally developed the tensegrity concept in 1948, in the form of a cylindrical tensegrity tower. Buckminster Fuller invented truncated spherical tensegrity modules in 1949 by incorporating Snelson's tensegrity concept into his geodesics (Marks and Fuller, 1973; Pugh, 1976; Kenner, 1976). The spherical tensegrity modules were developed from regular polyhedra by truncating all vertices. Resulting tensegrity modules were adopted to form lightweight deployable domes (Marks and Fuller, 1973). A construction method of truncated spherical tensegrity modules may be found in the book by Pugh (1976).

* Corresponding author. Tel.: +1-858-534-3821; fax: +1-858-534-4543.
E-mail address: murakami@mae.ucsd.edu (H. Murakami).

0020-7683/01/$ - see front matter © 2001 Elsevier Science Ltd. All rights reserved.
PII: S0020-7683(01)00030-0

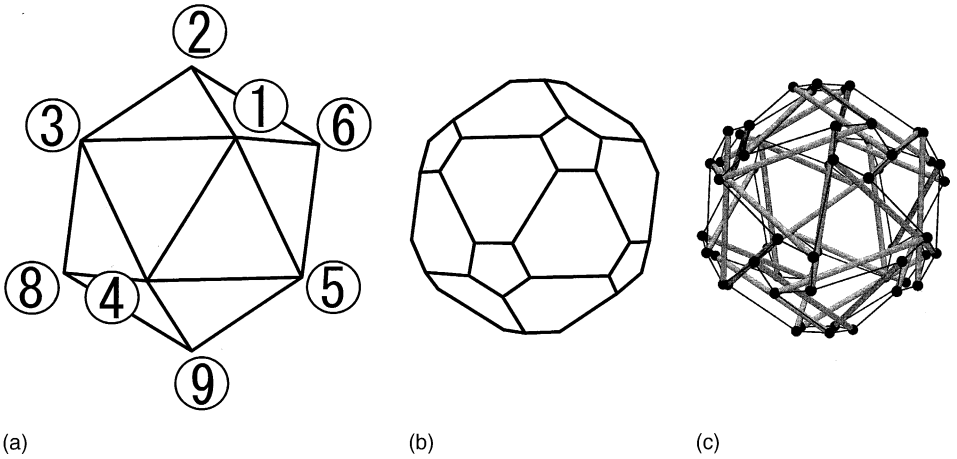

Fig. 1. (a) A regular icosahedron, (b) a regular truncated icosahedron, and (c) a regular truncated icosahedral tensegrity module.

Fig. 1a and b illustrate a regular icosahedron and a regular truncated icosahedron, respectively. The truncated icosahedron in Fig. 1b is formed by cutting off each vertex along a plane perpendicular to the radius emanating from the center of the icosahedron. The new faces become regular pentagons, referred to as truncating pentagons. Fig. 1c illustrates a truncated icosahedral tensegrity module. In Fig. 1c, thin lines denote cables, while thick lines represent bars. There is a one-to-one correspondence between the nodes and edges of a regular truncated icosahedron in Fig. 1b and the nodes and cables of the tensegrity module in Fig. 1c. This implies that the nodes and edges of the truncated icosahedron in Fig. 1b shows the connection of cables in Fig. 1c. In addition, five nodes of each truncating pentagon are connected to nodes of five adjacent truncating pentagons by using five bars. Further, the truncating pentagons of the tensegrity module can exist at a twisted state, i.e., each truncating pentagon is rotated by a twist angle α with respect to the radius through the truncated vertex. The tensegrity module achieves a stiff stable configuration only at a specific twist angle. The twist angle is unknown and has been found by trial-and-error experiments.

Fig. 2a and b illustrate, respectively, a regular dodecahedron and a regular truncated dodecahedron. The truncating faces form equilateral triangles. Fig. 2c illustrates a truncated dodecahedral tensegrity module. There is a one-to-one correspondence between the nodes and edges of the regular truncated dodecahedron

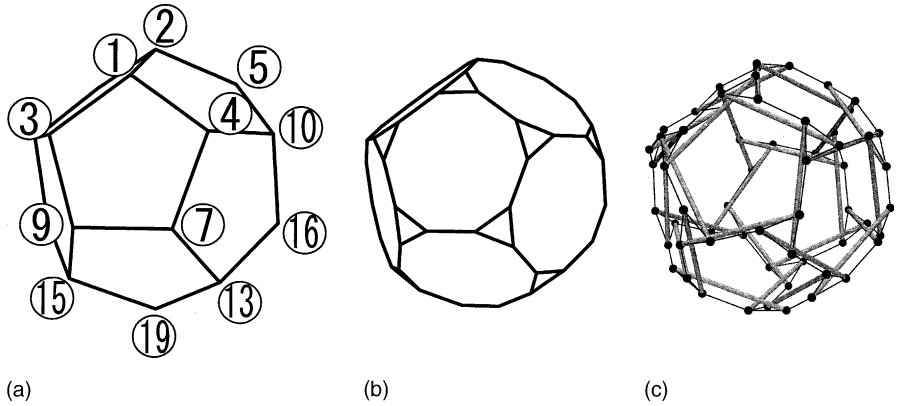

Fig. 2. (a) A regular dodecahedron, (b) a regular truncated dodecahedron, and (c) a regular truncated dodecahedral tensegrity module.

in Fig. 2b and the nodes and cables of the tensegrity module in Fig. 2c. Three nodes of each truncating triangle are connected to nodes of three adjacent triangles by using three bars.

It is noted that a regular icosahedron in Fig. 1a and a regular dodecahedron in Fig. 2a are dual. The center of each face of the icosahedron corresponds to a vertex of the dodecahedron. Conversely, the center of each face of the dodecahedron corresponds to a vertex of the icosahedron. Further, every congruent motion of one is a congruent motion of the other. All congruent motions of both regular icosahedrons and dodecahedrons form the icosahedral group A_5 (Ledermann, 1961; Grossman and Magnus, 1964).

In addition to man-made geodesic structures, regular truncated polyhedra and spherical tensegrity modules appear in nature. Ingber (1998) addressed assembly patterns of organic structures, such as cells, tissues, organs, and animals, and presented a set of examples of a universal building rule of self-assembly at different scales based upon geodesic tensegrity. Ingber also illustrated the effect of pre-stress in changing shapes and evolution of cells. If the truncation in Fig. 1b is done in such a way to form regular hexagonal and pentagonal faces, the patches of a soccer ball are obtained. The truncated icosahedron with a carbon atom at each vertex represents a carbon molecule: C_{60} (Curl and Smalley, 1988; Kroto, 1988). After Buckminster Fuller, chemists refer to this carbon molecule as the buckminsterfullerene or buckyball. Chung and Sternberg (1993) using group theory investigated the symmetric property of the buckyball.

Fuller's spherical tensegrity modules have been built and investigated qualitatively. However, quantitative static and dynamic analyses have not yet been performed on Fuller's spherical tensegrity modules. Analytical expressions for the twist angle are missing for defining the initial shape of any spherical tensegrity module. Since tensegrity structures are lightweight and flexible, they may be useful for controlling both shape and stiffness in real time. Skelton and Sultan (1997) first demonstrated the unique advantages achieved by controlling a two-stage cylindrical tensegrity module with three bars at each stage. Further, Sultan (1999) performed static and dynamic analyses of cylindrical tensegrity modules by extensively using a symbolic manipulator.

The first objective of the paper is to analytically find initial shapes and pre-stress modes for regular icosahedral and dodecahedral tensegrity modules in Figs. 1c and 2c. The second objective is to find natural frequencies and associated mode shapes for pre-stressed configurations to classify a large number of infinitesimal mechanism modes. To achieve the above objectives, a set of static and dynamic characterization procedures proposed by the authors was utilized. The authors previously applied the procedure to simple cylindrical tensegrity modules (Murakami, 2001a,b; Murakami and Nishimura, 1999, 2000). In what follows, the linear characterization procedure of tensegrity modules is first summarized.

2. Static and dynamic characterization procedures

A configuration of a truss with n_N nodes in Euclidean space $\mathbf{R}^3$ is described by the nodal coordinate $\mathbf{x}$ with respect to an inertial Cartesian coordinate frame $\{x, y, z\}$. By using a finite element (FE) kinematical representation, nodes of the structure are identified by the global node numbers, $1, 2, \ldots, n_N$. Truss elements are identified by element numbers, $1, 2, \ldots, n_E$ in parentheses, where n_E is the total number of truss elements. For a truss structure with n_E elements and n_N nodes with n_C linearly-independent displacement constraints, there are $n_V \equiv 3n_N - n_C$ unknown displacement components. Let the internal element-force vector be denoted by $\mathbf{s}$, an $n_E \times 1$ column matrix, and the external nodal-force vector by $\mathbf{f}$, an $n_V \times 1$ column matrix. The equilibrium equation for static loading $\mathbf{f}$ is expressed as:

$$\mathbf{A}\mathbf{s} = \mathbf{f}, \tag{1a}$$

where $\mathbf{A}$ is an $n_V \times n_E$ matrix consisting of direction cosines of truss elements. If a nontrivial internal element-force $\mathbf{s}$ exists without external forces, it must satisfy

$$\mathbf{As} = \mathbf{0}, \quad \mathbf{s} \neq \mathbf{0}. \tag{1b}$$

In the sequel, a nontrivial internal element-force $\mathbf{s}$ is referred to as a pre-stress mode.

Clark Maxwell (1864, 1890) classified the stiffness of truss structures by using the Maxwell number Mx:

$$Mx \equiv n_{\mathrm{E}} - n_{\mathrm{V}}. \tag{2}$$

According to Maxwell, when $Mx > 0$ (there are more columns than rows in $\mathbf{A}$), trusses are redundant and statically indeterminate. When $Mx = 0$ and the determinant of $\mathbf{A}$ is nonzero, trusses are statically determinate. When $Mx < 0$ (there are fewer number of columns than rows in $\mathbf{A}$), trusses become kinematically indeterminate mechanisms. As exceptions to the above for $Mx \leqslant 0$, Maxwell noted structures which exhibit "inferior order of stiffness", i.e., the stiffness is on the order of pre-stress, instead of on the order of Young's modulus.

Calladine (1978) investigated the algebraic structure of the linear transformation defined by Eq. (1a) applied to tensegrity structures. Calladine found the relationship between the number of pre-stress modes n_{S} and the number of infinitesimal mechanism modes n_{M} as follows (Pellegrino and Calladine, 1986):

$$n_{\mathrm{S}} - n_{\mathrm{M}} = Mx. \tag{3}$$

The first step in characterizing tensegrity modules is to compute the Maxwell number (2) and the number of infinitesimal mechanism modes for a pre-stress mode, $n_{\mathrm{S}} = 1$, by using Calladine's relation (3). In what follows, it will be shown that $Mx = -54$ for both icosahedral and dodecahedral tensegrity modules. These non-redundant modules collapse if all columns of $\mathbf{A}$ are linearly independent, i.e., rank $\mathbf{A} = n_{\mathrm{E}}$ and $n_{\mathrm{S}} = 0$. Non-redundant tensegrity modules exist only at pre-stressable configurations where rank $\mathbf{A} = n_{\mathrm{E}} - 1$ and $n_{\mathrm{S}} = 1$ (Murakami, 2001b). The second step is to analytically find a pre-stressable configuration with tension in cables and compression in bars.

Clapeyron's theorem (for example, Sokolnikoff, 1956) states that the work done by the external forces acting through the displacements from the natural configuration is equal to twice the strain energy of the body. Clapeyron's theorem yields:

$$\langle \mathbf{f}, \mathbf{d} \rangle_{n_{\mathrm{V}}} = \langle \mathbf{s}, \mathbf{e} \rangle_{n_{\mathrm{E}}}, \tag{4}$$

where $\mathbf{d}$ is the nodal displacement vector in $\mathbf{R}^{n_{\mathrm{V}}}$, $\mathbf{e}$ denotes the element elongation vector in $\mathbf{R}^{n_{\mathrm{E}}}$, and $\langle , \rangle_n$ denotes the inner product in $\mathbf{R}^n$. By substituting the linear transformation (1a) into Eq. (4) from the space of the internal element-forces $\mathbf{s}$ in $\mathbf{R}^{n_{\mathrm{E}}}$ to the external nodal-forces in $\mathbf{R}^{n_{\mathrm{V}}}$, one obtains the adjoint transformation $\mathbf{A}^{\mathrm{T}}$ from $\mathbf{R}^{n_{\mathrm{V}}}$ to $\mathbf{R}^{n_{\mathrm{E}}}$:

$$\langle \mathbf{As}, \mathbf{d} \rangle_{n_{\mathrm{V}}} \equiv \langle \mathbf{s}, \mathbf{A}^{\mathrm{T}}\mathbf{d} \rangle_{n_{\mathrm{E}}}. \tag{5}$$

In the sequel $\mathbf{A}^{\mathrm{T}}$ denotes the transpose of $\mathbf{A}$. This definition of the element elongation $\mathbf{e}$ agrees, as it should, with that obtained from the small deformation FE truss analyses:

$$\mathbf{e} = \mathbf{A}^{\mathrm{T}}\mathbf{d}. \tag{6}$$

The null space of the transformation $\mathbf{A}$ in Eq. (1b) is spanned by pre-stress modes, while the null space of the adjoint transformation $\mathbf{A}^{\mathrm{T}}$ in Eq. (6) is spanned by both infinitesimal mechanism modes and rigid-body modes. These modes do not cause any element elongation, $\mathbf{e} = \mathbf{0}$. If the structure is constrained against rigid body motion, the null space of the adjoint transformation $\mathbf{A}^{\mathrm{T}}$ is spanned by infinitesimal mechanism modes only.

In order to investigate the stiffening effect by a pre-stress mode, modal analyses may be conducted by utilizing the equations of motion linearized at a pre-stressed configuration. Let Young's modulus, the area of cross section, the element length, and the second Piola–Kirchhoff stress at the pre-stressed state be denoted respectively by Y_0, A_0, l_0, and S_{11}. In terms of a harmonically vibrating nodal displacement vector

$\mathbf{d} = \tilde{\mathbf{d}}\exp(\mathrm{i}\omega t)$ with the amplitude $\tilde{\mathbf{d}}$, the angular velocity ω, and time t, the generalized eigen problem becomes

$$\mathbf{K}_{\mathrm{T}}\tilde{\mathbf{d}} = \omega^2\mathbf{M}\tilde{\mathbf{d}}, \tag{7a}$$

where $\mathbf{K}_{\mathrm{T}}$ and $\mathbf{M}$ are the tangent stiffness and mass matrices. The tangent stiffness matrix $\mathbf{K}_{\mathrm{T}}$ is an $n_{\mathrm{V}} \times n_{\mathrm{V}}$, positive semi-definite, symmetric matrix and becomes a positive definite matrix if rigid body modes are constrained. The mass matrix is an $n_{\mathrm{V}} \times n_{\mathrm{V}}$, positive definite, symmetric matrix. The stiffness matrix $\mathbf{K}_{\mathrm{T}}$ is decomposed into the initial stiffness $\mathbf{K}_0$, employed for small-deformation truss analyses, and the stiffness $\mathbf{K}_{\mathrm{s}}$ induced by a pre-stress mode:

$$\mathbf{K}_{\mathrm{T}} = \mathbf{K}_0 + \mathbf{K}_{\mathrm{s}}. \tag{7b}$$

If one relates the global displacement vector $\mathbf{d}$ to the elemental displacement vector $\mathbf{d}^{(e)}$ of element (e) by a Boolean map $\mathbf{L}g^{(e)}$, a $6 \times n_{\mathrm{V}}$ matrix, $\mathbf{K}_0$ and $\mathbf{K}_{\mathrm{s}}$ are defined by the 6×6 elemental matrices $\mathbf{K}_0^{(e)}$ and $\mathbf{K}_{\mathrm{s}}^{(e)}$ as:

$$\mathbf{K}_0 = \sum_{e=1}^{n_{\mathrm{E}}} \mathbf{L}g^{(e)^{\mathrm{T}}}\mathbf{K}_0^{(e)}\mathbf{L}g^{(e)}, \tag{7c}$$

$$\mathbf{K}_{\mathrm{s}} = \sum_{e=1}^{n_{\mathrm{E}}} \mathbf{L}g^{(e)^{\mathrm{T}}}\mathbf{K}_{\mathrm{s}}^{(e)}\mathbf{L}g^{(e)}, \tag{7d}$$

where

$$\mathbf{K}_0^{(e)} = \left(\frac{Y_0 A_0}{l_0}\right)^{(e)} \begin{bmatrix} \mathbf{G}\mathbf{G}^{\mathrm{T}} & -\mathbf{G}\mathbf{G}^{\mathrm{T}} \\ -\mathbf{G}\mathbf{G}^{\mathrm{T}} & \mathbf{G}\mathbf{G}^{\mathrm{T}} \end{bmatrix}^{(e)}, \tag{7e}$$

$$\mathbf{K}_{\mathrm{s}}^{(e)} = \left(\frac{S_{11} A_0}{l_0}\right)^{(e)} \begin{bmatrix} \mathbf{I}_3 & -\mathbf{I}_3 \\ -\mathbf{I}_3 & \mathbf{I}_3 \end{bmatrix}, \tag{7f}$$

in which $\mathbf{G}^{(e)}$ is the direction cosine of element (e) and $\mathbf{I}_3$ is a 3×3 identity matrix. It is observed that the pre-stress stiffening in Eqs. (7d) and (7f) is "isotropic" at each node (Argyris and Scharpf, 1972; Murakami, 2001a). In the sequel, the above equations will be utilized to characterize static and dynamic response of Fuller's spherical tensegrity modules.

3. Regular truncated icosahedral tensegrity modules

3.1. Maxwell number and the number of infinitesimal mechanisms

In order to define the Maxwell number of tensegrity modules, it is necessary to count the number of nodes, the number of bars, and the number of cables. The Euler characteristic for polyhedra in three-dimensional space is useful for finding these numbers (Sternberg, 1993; Frankel, 1997). The Euler characteristic relates the number of faces f, the number of vertices v, and the number of edges e as:

$$f - e + v = 2. \tag{8}$$

The regular icosahedron, shown in Fig. 1a, consists of twelve vertices ($v = 12$) and 20 equilateral triangular faces ($f = 20$). Five triangles meet at each vertex. Euler's relation (8) yields 30 edges, $e = 30$.

If one truncates the icosahedron by cutting off each vertex along a plane perpendicular to the radius through the vertex, the new faces created become a set of regular pentagons. The truncated icosahedral tensegrity module has the same number of nodes as the truncated regular icosahedron. Therefore, the

Table 1
Basic properties of truncated icosahedral and dodecahedral tensegrity modules

n_N	n_E	Mx	n_M	n_S
60	120	−54	55	1

number of nodes of the tensegrity module becomes $n_N = 5 \times 12 = 60$. Since bars connect 60 nodes, there are 30 bars. Further, the connection of cables is the same as the edges of the truncated icosahedron in Fig. 1b. As a result, there are 30 vertical cables along the edges of the regular icosahedron and 5×12 cables along the edges of truncating pentagons.

Thus the number of truss elements become $n_E = 30 + 30 + 60 = 120$. The Maxwell number (2) of a truncated icosahedral tensegrity module is $Mx = 120 - (3 \times 60 - 6) = -54$. Calladine's relation (3) with $n_S = 1$ shows that the tensegrity possesses 55 infinitesimal mechanism modes, i.e., $n_M = 55$. Those numbers are compiled in Table 1. The truncated icosahedral tensegrity module in Fig. 1c consists of cables and bars. The connection of cables is identical to the edges of the regular truncated icosahedron in Fig. 1b. In the tensegrity module, each truncating pentagon only exists at a twisted state with respect to the radius through the truncated vertex.

3.2. Initial shape finding

Fuller's spherical tensegrity modules have three cables and one bar at each node. In order to find the twist angle, it is necessary to impose the existence condition of a pre-stress mode on the initial equilibrium matrix **A** in Eq. (1b). To form **A**, nodal coordinates must be analytically computed for an unknown twist angle α. In order to define nodal coordinates, the congruent motions of a regular icosahedron become extremely helpful. There are 60 congruent configurations of a regular icosahedron. They form the icosahedral group A_5, i.e., the alternating group of five symbols (Ledermann, 1961; Grossman and Magnus, 1964). The icosahedral group also describes the congruent motions of both a regular truncated icosahedron and a regular truncated icosahedral tensegrity module. The congruent motions of a regular icosahedron in Fig. 1a are described by the products of two generators: the rotation by $2\pi/5$ with respect to a diagonal joining two opposite vertices and the flip by π with respect to a median defined by connecting the centers of two facing edges. In the sequel they are referred to as **R** and **F**, respectively.

There are 15 medians since there are 30 edges in a regular icosahedron in Fig. 1a. The 15 medians comprise five sets of orthogonal triads (Grossman and Magnus, 1964). A set of orthogonal medians is selected as the body-fixed Cartesian x'-, y'-, and z'- axes, as well as the inertial Cartesian x-, y-, and z-axes, as illustrated in Fig. 3. In the figure, both coordinate frames coincide. However, as **R** and **F** are applied, the body-fixed frame $\{x', y', z'\}$ rotates with the icosahedron while the inertial frame $\{x, y, z\}$ remains stationary.

Let the edge length of a regular icosahedron be denoted by b. The edges of the regular icosahedron intercept the coordinate axes at $\pm(1 + \sqrt{5})b/4$, as illustrated in Fig. 3. Let the length of the truncated edges be denoted by a. The edge length of the truncating regular pentagons becomes a. The ratio $h \equiv a/b$ is referred to as the truncation ratio. Fig. 3 also shows the positive direction of the twist angle with respect to truncating regular pentagon 1′-2′-3′-4′-5′ twisted in the "clockwise direction" by α to become regular pentagon 1-2-3-4-5. The rotation **R** with respect to the radius through vertex 1 is described by the axis $\mathbf{u}'$:

$$\mathbf{u}' = \left[\frac{\sqrt{2}}{\sqrt{5+\sqrt{5}}}, \quad 0, \quad \frac{1+\sqrt{5}}{\sqrt{2}\sqrt{5+\sqrt{5}}} \right]^{\mathrm{T}}$$

with respect to the body-fixed frame $\{x', y', z'\}$ and the rotation angle $\phi = 2\pi/5$ in the "counterclockwise direction". By using the Euler parameters for $\phi = 2\pi/5$ (Haug, 1989):

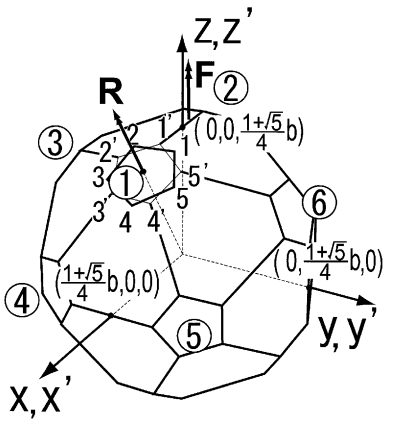

Fig. 3. A body-fixed Cartesian coordinate system $\{x',y',z'\}$ and the inertial Cartesian coordinate system $\{x,y,z\}$ erected for a regular truncated icosahedron.

$$e_0 = \cos\frac{\phi}{2}, \quad e_1 = \frac{\sqrt{2}}{\sqrt{5+\sqrt{5}}}\sin\frac{\phi}{2}, \quad e_2 = 0, \quad e_3 = \frac{1+\sqrt{5}}{\sqrt{2}\sqrt{5+\sqrt{5}}}\sin\frac{\phi}{2}, \tag{9a}$$

the rotation matrix $\mathbf{R}$ with respect to the body-fixed frame is defined as follows:

$$\mathbf{R} = 2\begin{bmatrix} e_0^2+e_1^2-\frac{1}{2} & -e_0e_3 & e_1e_3 \\ e_0e_3 & e_0^2-\frac{1}{2} & -e_0e_1 \\ e_1e_3 & e_0e_1 & e_0^2+e_3^2-\frac{1}{2} \end{bmatrix}. \tag{9b}$$

The flip $\mathbf{F}$ with respect to the z'-axis by π is defined by the Euler parameters:

$$e_0 = e_1 = e_2 = 0, \quad e_3 = 1, \tag{10a}$$

which defines the flip matrix with respect to $\{x',y',z'\}$ as:

$$\mathbf{F} = \begin{bmatrix} -1 & 0 & 0 \\ 0 & -1 & 0 \\ 0 & 0 & 1 \end{bmatrix}. \tag{10b}$$

Fig. 4a shows a graph or a Cayley diagram of the icosahedral group A_5 which represents all congruent motions of a regular icosahedron, shown in Fig. 1a (Grossman and Magnus, 1964). In the graph, nodes represent different configurations of a regular icosahedron and edges represent congruent motions. Solid lines with arrows indicate $\mathbf{R}$ with respect to $\mathbf{u}'$ by $\phi = 2\pi/5$ and dashed lines denote $\mathbf{F}$ with respect to the z'-axis. Let the identity of the group be denoted by $\mathbf{I}$. The generators $\mathbf{R}$ and $\mathbf{F}$ satisfy the following relations:

$$\mathbf{RRRRR} = \mathbf{I}, \quad \mathbf{FF} = \mathbf{I}, \quad \mathbf{FRFRFR} = \mathbf{I}. \tag{11}$$

The above group operations are expressed by matrix multiplications, i.e., the operators are applied from the right to the left. Further, the inverse of $\mathbf{R}$ and $\mathbf{F}$ are

$$\mathbf{R}^{-1} = \mathbf{R}^{\mathrm{T}}, \quad \mathbf{F}^{-1} = \mathbf{F}. \tag{12}$$

The graph of the icosahedral group will be used: (i) to generate all nodal coordinates of the tensegrity module starting from the coordinates of node 1 of the twisted regular pentagon 1-2-3-4-5 in Fig. 3 and (ii) to define the connections of cable elements.

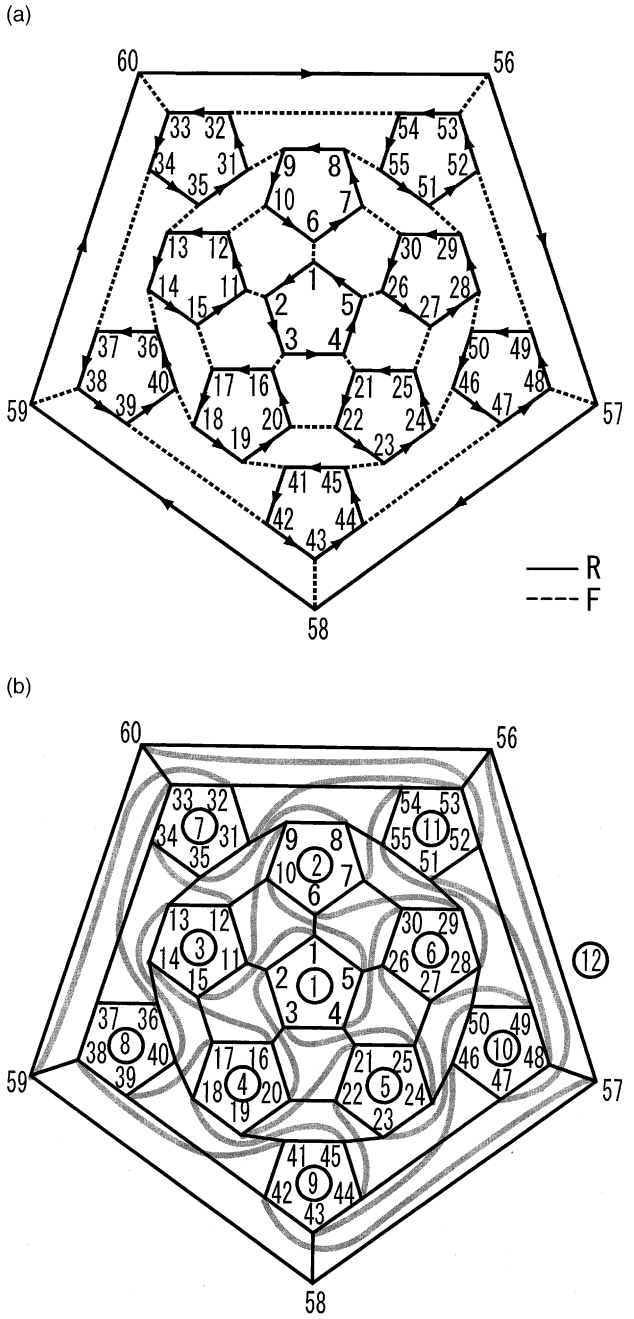

Fig. 4. (a) A graph of the icosahedral group and (b) a connectivity diagram of a truncated icosahedral tensegrity module with a positive twist angle (thick lines denote bar connections).

If the nodal coordinates of node 1 are given, by following the lines in Fig. 4a and performing the **R** or **F** operations one can move node 1 to any node identified at the original configuration. For example, node 1

can be moved to node 5 position by **RRRR** or $\mathbf{R}^{\mathrm{T}}$ as shown in Fig. 4a. To move node 1 to node 6, one operates **F**. The motion of node 1 to node 15 is achieved by multiplying $\mathbf{R}^{\mathrm{T}}\mathbf{F}\mathbf{R}$.

It is noted that the number of congruent configurations is the same as the number of nodes of both the truncated icosahedron in Fig. 1b and the tensegrity module in Fig. 1c. In order to take advantage of the above coincidence between the nodes of the tensegrity module and the congruent configurations of the icosahedral group, node numbers are assigned to the nodes of the graph in Fig. 4a.

An examination of cable connections of the tensegrity module reveals that there is a one-to-one correspondence between cable elements and edges of the truncated icosahedron in Fig. 1b. Further, the edges of the truncated icosahedron in Fig. 1b have a one-to-one correspondence with the paths of the graph in Fig. 4a. Therefore, the paths of the graph show the connection of cables of truncated icosahedral tensegrity modules.

A connectivity diagram of tensegrity elements is shown for a positive twist angle α in Fig. 4b. The connection of bars is illustrated by thick free-hand curves. In Fig. 4b, the truncated vertex of the regular icosahedron identifies each truncating pentagon. For a negative α the connection of cables is identical to that in Fig. 4b. However, the connection of bars become the mirror image with respect to the axis connecting nodes 1 and 6. In the sequel, the analysis will be performed for positive values of α.

The description of group theory does not require any coordinate system (Ledermann, 1961). However, subsequent analyses based upon Newtonian physics is performed with respect to the inertial Cartesian frame $\{x,y,z\}$. In order to compute nodal coordinates with respect to the inertial frame $\{x,y,z\}$, one must keep track of the orientation of the body-fixed frame $\{x',y',z'\}$ with respect to the inertial frame $\{x,y,z\}$ at each **R** or **F** operation. In the sequel, therefore, a shortcut is made in generating nodal coordinates with respect to the inertial frame $\{x,y,z\}$. Let the position vector of node i be denoted by r_i. The coordinates of node $1'$ of pentagon $1'$-$2'$-$3'$-$4'$-$5'$ are defined with respect to the inertial frame $\{x,y,z\}$ as:

$$\mathbf{r}_{1'} = b\left[\tfrac{1}{2} - h, \quad 0, \quad \tfrac{\sqrt{5}+1}{4}\right]^{\mathrm{T}}, \tag{13a}$$

where $h \equiv a/b$ denotes the truncation ratio.

By rotating $\mathbf{r}_{1'}$ with

$$\mathbf{u} = \left[\frac{\sqrt{2}}{\sqrt{5+\sqrt{5}}}, \quad 0, \quad \frac{1+\sqrt{5}}{\sqrt{2}\sqrt{5+\sqrt{5}}}\right]^{\mathrm{T}},$$

rather than $\mathbf{u}'$, by $\phi = -\alpha$ in Eqs. (9a) and (9b) as shown in Fig. 3 the coordinates of node 1 are obtained.

$$\mathbf{r}_1 = b\begin{Bmatrix} \frac{1}{2} - \frac{h}{10}\{5 - \sqrt{5} + (5+\sqrt{5})\cos\alpha\} \\ \frac{h}{\sqrt{10}}\sqrt{5+\sqrt{5}}\sin\alpha \\ \frac{1+\sqrt{5}}{4} - \frac{h}{\sqrt{5}}(1-\cos\alpha) \end{Bmatrix}. \tag{13b}$$

Let the rotation with respect to **u** by $2\pi/5$ with respect to the inertial frame be denoted by $\mathbf{R}_{\mathrm{G}}$ and the flip with respect to the z-axis be denoted by $\mathbf{F}_{\mathrm{G}}$. The coordinates of nodes 2, 3, 4, 5, 6, and 15 can easily be computed by

$$\mathbf{r}_2 = \mathbf{R}_{\mathrm{G}}\mathbf{r}_1, \quad \mathbf{r}_3 = \mathbf{R}_{\mathrm{G}}\mathbf{r}_2, \quad \mathbf{r}_4 = \mathbf{R}_{\mathrm{G}}\mathbf{r}_3, \quad \mathbf{r}_5 = \mathbf{R}_{\mathrm{G}}\mathbf{r}_4, \tag{13c–f}$$

$$\mathbf{r}_6 = \mathbf{F}_{\mathrm{G}}\mathbf{r}_1, \quad \mathbf{r}_{15} = \mathbf{R}_{\mathrm{G}}\mathbf{F}_{\mathrm{G}}\mathbf{r}_5. \tag{13g,h}$$

For remaining nodes, the operations by using $\mathbf{R}_{\mathrm{G}}$ and $\mathbf{F}_{\mathrm{G}}$ are summarized in Appendix A.

The nodal coordinates necessary for subsequent analyses are

$$\mathbf{r}_2 = b\begin{Bmatrix} \frac{1}{2}+\frac{h}{40}\{-20+4\sqrt{5}(1-\cos\alpha)-\sqrt{2}\sqrt[3]{5+\sqrt{5}}\sin\alpha)\} \\ -\frac{h}{40}\{10(1+\sqrt{5})\cos\alpha+(-5+\sqrt{5})\sqrt{2}\sqrt{5+\sqrt{5}}\sin\alpha\} \\ \frac{\sqrt{5}+1}{4}+\frac{h}{20}\{(5-\sqrt{5})\cos\alpha+\sqrt{5}(-4+\sqrt{2}\sqrt{5+\sqrt{5}}\sin\alpha)\} \end{Bmatrix}, \tag{14a}$$

$$\mathbf{r}_5 = b\begin{Bmatrix} \frac{1}{2}+\frac{h}{40}\{-20+4\sqrt{5}(1-\cos\alpha)+\sqrt{2}\sqrt[3]{5+\sqrt{5}}\sin\alpha\} \\ \frac{h}{40}\{10(1+\sqrt{5})\cos\alpha+(5-\sqrt{5})\sqrt{2}\sqrt{5+\sqrt{5}}\sin\alpha\} \\ \frac{\sqrt{5}+1}{4}+\frac{h}{20}\{(5-\sqrt{5})\cos\alpha-\sqrt{5}(4+\sqrt{2}\sqrt{5+\sqrt{5}}\sin\alpha)\} \end{Bmatrix}, \tag{14b}$$

$$\mathbf{r}_6 = b\begin{Bmatrix} -\frac{1}{2}+\frac{h}{10}\{5-\sqrt{5}+(5+\sqrt{5})\cos\alpha\} \\ -\frac{h}{\sqrt{10}}\sqrt{5+\sqrt{5}}\sin\alpha \\ \frac{\sqrt{5}+1}{4}-\frac{h}{\sqrt{5}}(1-\cos\alpha) \end{Bmatrix}, \tag{14c}$$

$$\mathbf{r}_{15} = b\begin{Bmatrix} \frac{h}{40}\{10(1+\sqrt{5})\cos\alpha+(-5+\sqrt{5})\sqrt{2}\sqrt{5+\sqrt{5}}\sin\alpha\} \\ -\frac{\sqrt{5}+1}{4}+\frac{h}{20}\{(-5+\sqrt{5})\cos\alpha+\sqrt{5}(4-\sqrt{2}\sqrt{5+\sqrt{5}}\sin\alpha)\} \\ \frac{1}{2}+\frac{h}{40}\{-20+4\sqrt{5}(1-\cos\alpha)-\sqrt{2}\sqrt[3]{5+\sqrt{5}}\sin\alpha\} \end{Bmatrix}. \tag{14d}$$

It is noted that the paths in Fig. 4a are neatly identified by the rotation $\mathbf{R}$ and $\mathbf{F}$ with respect to the body-fixed frame $\{x', y', z'\}$. With respect to the inertial frame $\{x, y, z\}$, however, the paths are described by more complicated combinations of $\mathbf{R}_G$ and $\mathbf{F}_G$. For example, node 1 is moved to node 10 by $\mathbf{F}_G\mathbf{R}_G^T$ instead of the product $\mathbf{R}^T\mathbf{F}$.

At this stage, the nodal coordinates of the truncated icosahedral tensegrity module are all defined with respect to the inertial frame $\{x, y, z\}$ and the connections of elements are defined as shown in Fig. 4b. One can easily construct the initial equilibrium matrix $\mathbf{A}$, a $3n_N \times n_E$ matrix, in Eq. (1b) for an unknown twist angle α. The initial equilibrium matrix without constraining rigid-body modes is a 180×120 rectangular matrix. The tensegrity module becomes an unstable mechanism if there is no pre-stress mode which spans the null space of the linear transformation $\mathbf{A}$. The twist angle α is found by imposing the existence of a nontrivial pre-stress-mode $\mathbf{s}$ on Eq. (1b):

$$\det\left(\mathbf{A}^T\mathbf{A}\right) = 0. \tag{15}$$

The matrix $\mathbf{A}^T\mathbf{A}$ becomes a 120×120 matrix. It is not possible to analytically compute the above determinant for an unknown twist angle α. Therefore, a straightforward application of Eq. (15) to the tensegrity modules yields only numerical solutions for α after solving the nonlinear Eq. (15). In order to alleviate the difficulty in obtaining an analytical solution for α, the spherical symmetry of the tensegrity module defined by congruent motions is utilized.

Since a regular icosahedron, a regular truncated icosahedron, and a regular truncated icosahedral tensegrity module in Fig. 1a–c possess the same congruent motions, it is natural to assume that the tensegrity elements in the same family possess the same pre-stress. There are only three families of tensegrity elements including bars, vertical cables, and truncating-edge cables. Therefore, the unknown element forces reduce to $\mathrm{s}' \equiv \{s_b\ s_v\ s_t\}^T$, where s_b, s_v, and s_t respectively denote element forces of bars, vertical cables, and truncating-edge cables. Let the equilibrium equation at node 1 be expressed as follows:

$$\mathbf{A}_1\mathbf{s}' = \mathbf{0}, \tag{16}$$

where $\mathbf{A}_1$ is a 3×3 matrix. The columns of $\mathbf{A}_1$ consist of the direction cosines of the bar and cables emanating from node 1. It is noted that if local frames are erected at nodes by rotating the local frame at node 1 according to the congruent motions shown in Fig. 4a, the same equilibrium equations (16) hold at all nodes.

In the sequel, it will be shown that under the assumption of the same element forces for the same family of elements, the existence condition (15) of a nontrivial pre-stress mode reduces to

$$\det \mathbf{A}_1 = 0. \tag{17}$$

The above simple equation is feasible for analytical solutions for both the twist angle and the pre-stress mode. Let the congruent rotation from node 1 to node i be denoted by $\mathbf{O}_i$ with respect to the inertial frame $\{x, y, z\}$. For example, $\mathbf{O}_2 = \mathbf{R}_G$, $\mathbf{O}_3 = \mathbf{R}_G\,\mathbf{R}_G$, and $\mathbf{O}_{10} = \mathbf{F}_G\mathbf{R}_G^T$. Since $\mathbf{O}_i$ is an orthogonal transformation matrix, $\mathbf{O}_i^T\mathbf{O}_i = \mathbf{I}$ (= identity matrix). The equilibrium equations (1b) for three element forces reduce to:

$$\begin{bmatrix} \mathbf{A}_1 \\ \mathbf{O}_2\mathbf{A}_1 \\ \vdots \\ \mathbf{O}_{n_N}\mathbf{A}_1 \end{bmatrix} \mathbf{s}' = \mathbf{0}. \tag{18a}$$

Eq. (15) with Eq. (18a) becomes

$$n_N \det(\mathbf{A}_1^T\mathbf{A}_1) = n_N \det \mathbf{A}_1 \det \mathbf{A}_1^T = 0, \tag{18b}$$

where n_N ($\neq 0$) is the number of nodes of the tensegrity module. Under the assumption of the same element forces for the same family of elements, Eqs. (17) and (18b) are equivalent since $\det \mathbf{A}_1^T = \det \mathbf{A}_1$.

Let the lengths of bars, vertical cables, and truncating-edge cables be denoted by l_b, l_v, and l_t, respectively. They are defined as follows:

$$l_b = \|\mathbf{r}_{15} - \mathbf{r}_1\|, \quad l_v = \|\mathbf{r}_6 - \mathbf{r}_1\|, \quad l_t = \|\mathbf{r}_2 - \mathbf{r}_1\|, \tag{19}$$

where $\mathbf{r}_1$, $\mathbf{r}_2$, $\mathbf{r}_6$, and $\mathbf{r}_{15}$ are defined in Eqs. (13b) and (14a)–(14d).

From the connectivity diagram in Fig. 4b the equilibrium equations at node 1 become

$$(\mathbf{r}_{15} - \mathbf{r}_1)\frac{s_b}{l_b} + (\mathbf{r}_6 - \mathbf{r}_1)\frac{s_v}{l_v} + (\mathbf{r}_2 - \mathbf{r}_1 + \mathbf{r}_5 - \mathbf{r}_1)\frac{s_t}{l_t} = \mathbf{0}. \tag{20}$$

A nontrivial solution $\{s_b/l_b\ s_v/l_v\ s_t/l_t\}^T$ exists when

$$\begin{aligned} h^2\Big[&8(-3+\sqrt{5})\cos^3\alpha + 4\Big\{4(\sqrt{5}-2) - (\sqrt{5}-1)\sqrt{2}\sqrt{5+\sqrt{5}}\sin\alpha\Big\}\cos^2\alpha + \Big\{4(\sqrt{5}-1) \\ &+ 4(-3+\sqrt{5})\sqrt{2}\sqrt{5+\sqrt{5}}\sin\alpha\Big\}\cos\alpha - 4\sqrt{2}\sqrt{5+\sqrt{5}}(3\sqrt{5}-7)\sin\alpha - 8\sqrt{5}\Big] \\ &+ h\Big\{4(5-3\sqrt{5})\cos^2\alpha + (5-\sqrt{5})(8+2\sqrt{2}\sqrt{5+\sqrt{5}}\sin\alpha)\cos\alpha \\ &+ 8\sqrt{2}\sqrt{5+\sqrt{5}}(-5+2\sqrt{5})\sin\alpha + 10(1+\sqrt{5})\Big\} - 20\cos\alpha + 5(3-\sqrt{5})\sqrt{2}\sqrt{5+\sqrt{5}}\sin\alpha = 0, \end{aligned} \tag{21}$$

with the eigenmode

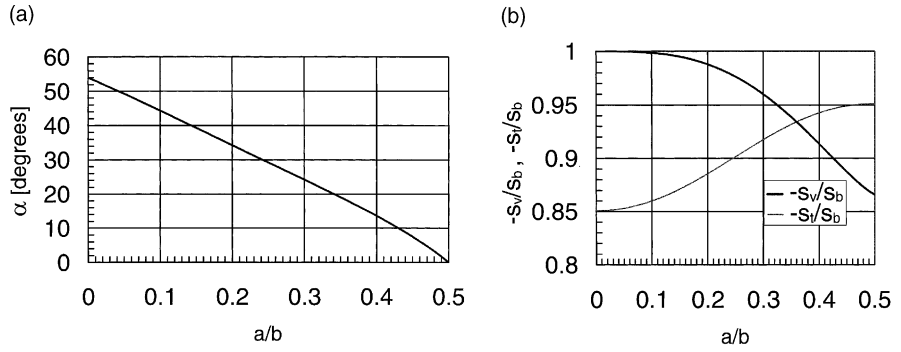

Fig. 5. (a) The twist angle α versus the truncation ratio $h(\equiv a/b)$ for regular truncated icosahedral tensegrity modules and (b) the pre-stress mode versus the truncation ratio h for regular truncated icosahedral tensegrity modules.

$$\frac{s_v}{l_v} = -\frac{s_b}{l_b}\frac{5(\sqrt{5}-1)+h\{10-6\sqrt{5}+(-5+\sqrt{5})\cos\alpha+\sqrt{10}\sqrt{5+\sqrt{5}}\sin\alpha\}}{5(\sqrt{5}-1)+2h(5-3\sqrt{5}-2\sqrt{5}\cos\alpha)}, \tag{22a}$$

$$\frac{s_t}{l_t} = -\frac{s_b}{l_b}\frac{10(\sqrt{5}-1)+h\{20-12\sqrt{5}(1-\cos\alpha)+\sqrt{2}\sqrt[3]{5+\sqrt{5}}\sin\alpha\}}{20h(\sqrt{5}-1)\cos\alpha}. \tag{22b}$$

Eq. (21) yields the relation between the twist angle α and the truncation ratio $h \equiv a/b$. Fig. 5a shows the variation of α as a function of the truncation ratio h. As $h \to 0$ the twist angle α becomes $3\pi/10$ ($= 54°$), while as $h \to \frac{1}{2}$, α tends to zero. The corresponding pre-stress mode: $\{-s_t/s_b,\ -s_v/s_b\}$ is plotted in Fig. 5b. The pre-stress modes in Eqs. (22a) and (22b) take tension in cables and compression in bars, i.e., $s_v > 0$ and $s_t > 0$ if $s_b < 0$. The optimum truncation ratio is found at $h = 0.36$ and $\alpha = 18°$ where the maximum value of the cable tension becomes minimum with $s_t = s_v$. Further, the maximum value of the cable tension is always less than the absolute value of bar compression.

By computing a full initial equilibrium matrix $\mathbf{A}$ for a prestressable configuration, one could easily obtain the eigenmodes corresponding to zero eigenvalue of $\mathbf{A}\mathbf{A}^T$ and identify 55 infinitesimal mechanism modes. However, the computation of infinitesimal mechanism modes was bypassed in lieu of the following modal analyses.

3.3. Modal analyses of regular truncated icosahedral tensegrity modules

For a prescribed bar force s_b and the twist angle $\alpha = 30°$, the initial element-forces due to pre-stress are completely defined by Eqs. (22a) and (22b). Modal analyses defined in Eqs. (7a)–(7f) were conducted for pre-stressed configurations with increasing amplitudes of pre-stress. For the subsequent numerical examples, steel bars and cables with Young's modulus $Y_0 = 200$ GPa and mass density $\rho = 7860$ kg/m^3 are considered. The diameter of cables is 0.003 m. Bars are hollow circular cylinders with outer and inner radii, 0.011 and 0.009 m, respectively. The length of bars is $l_b = 0.5$ m.

Results of the modal analyses are summarized in Table 2. Included are 18 lowest natural frequencies in Hz. The first 15 natural frequencies are associated with 55 infinitesimal mechanism modes. Their algebraic multiplicities, shown in parentheses, are also included in Table 2. The natural frequencies of infinitesimal mechanism modes, whose stiffness is due to pre-stress, increase proportionally to the square root of the amplitude of pre-stress, as seen in Eq. (7f). The natural frequencies higher than the 15th correspond to

Table 2
Natural frequencies in Hz and algebraic multiplicities of regular truncated icosahedral tensegrity modules for increasing pre-stress amplitudes

$\|s_b\|$	10(N)	50(N)	100(N)	500(N)	1000(N)
1st	1.69(5)	3.77(5)	5.33(5)	11.92(5)	16.85(5)
2nd	2.01(3)	4.50(3)	6.37(3)	14.24(3)	20.12(3)
3rd	2.29(1)	5.13(1)	7.25(1)	16.21(1)	22.92(1)
4th	2.87(3)	6.41(3)	9.06(3)	20.26(3)	28.64(3)
5th	2.94(5)	6.58(5)	9.31(5)	20.80(5)	29.41(5)
6th	3.74(4)	8.36(4)	11.83(4)	26.45(4)	37.40(4)
7th	3.96(5)	8.84(5)	12.51(5)	27.97(5)	39.55(5)
8th	4.08(4)	9.12(4)	12.90(4)	28.82(4)	40.73(4)
9th	4.19(5)	9.37(5)	13.25(5)	29.62(5)	41.88(5)
10th	4.20(3)	9.38(3)	13.27(3)	29.67(3)	41.96(3)
11th	4.21(4)	9.41(4)	13.30(4)	29.74(4)	42.06(4)
12th	4.45(3)	9.96(3)	14.08(3)	31.49(3)	44.53(3)
13th	4.69(3)	10.50(3)	14.84(3)	33.19(3)	46.94(3)
14th	6.48(4)	14.49(4)	20.49(4)	45.79(4)	64.71(4)
15th	7.36(3)	16.45(3)	23.27(3)	52.03(3)	73.57(3)
16th	316.76(3)	316.90(3)	317.08(3)	318.47(3)	320.21(3)
17th	436.65(5)	436.72(5)	436.82(5)	437.58(5)	438.53(5)
18th	495.29(4)	495.39(4)	495.51(4)	496.50(4)	497.74(4)

deformation modes (6) with nonzero element elongation. Therefore, in Table 2, the 16th and higher natural frequencies do not change significantly with increasing pre-stress amplitudes.

Fig. 6a–c show the first mode shape exhibiting an ellipsoidal deformation. There are five modes associated with the first natural frequency. The axes of the ellipsoids coincide with those of an orthogonal triad formed by medians. There are 15 medians in a regular icosahedron and form five sets of orthogonal triads. Therefore, the algebraic multiplicity of five for the first natural frequency is due to the symmetry with five sets of orthogonal medians. Fig. 6d–f illustrate the second mode in which a pair of opposing pentagons moves vertically. There are three modes associated with the second natural frequency. The third mode shown in Fig. 6g–i becomes the spherically symmetric mode without any multiplicity. The mode shapes and number of modes remain essentially the same even if the twist angles were considerably changed, except for minor switching of the orders of higher frequency modes.

The above modal analyses identify subspaces spanned by various infinitesimal mechanism modes based upon natural frequencies. Understanding mode shapes allows control engineers to choose loading points to excite desired infinitesimal mechanism modes. The infinitesimal mechanism modes associated with the first natural frequency have the least stiffness. Therefore, they require the least work to excite the modes. Due to space limitations, nonlinear stiffening of the tensegrity modules due to large deformation is deferred to subsequent publications. The authors presented nonlinear analyses for simple cylindrical tensegrity-modules (Murakami, 2001b; Murakami and Nishimura, 1999, 2000). In the next section, the dual tensegrity module is considered.

4. Regular truncated dodecahedral tensegrity modules

4.1. Maxwell number and the number of infinitesimal mechanisms

Fig. 2a illustrates a regular dodecahedron with 20 vertices and 12 regular pentagonal faces. Three regular pentagons meet at each vertex. Euler's relation (8) yields that there are 30 edges in Fig. 2a and 30 vertical

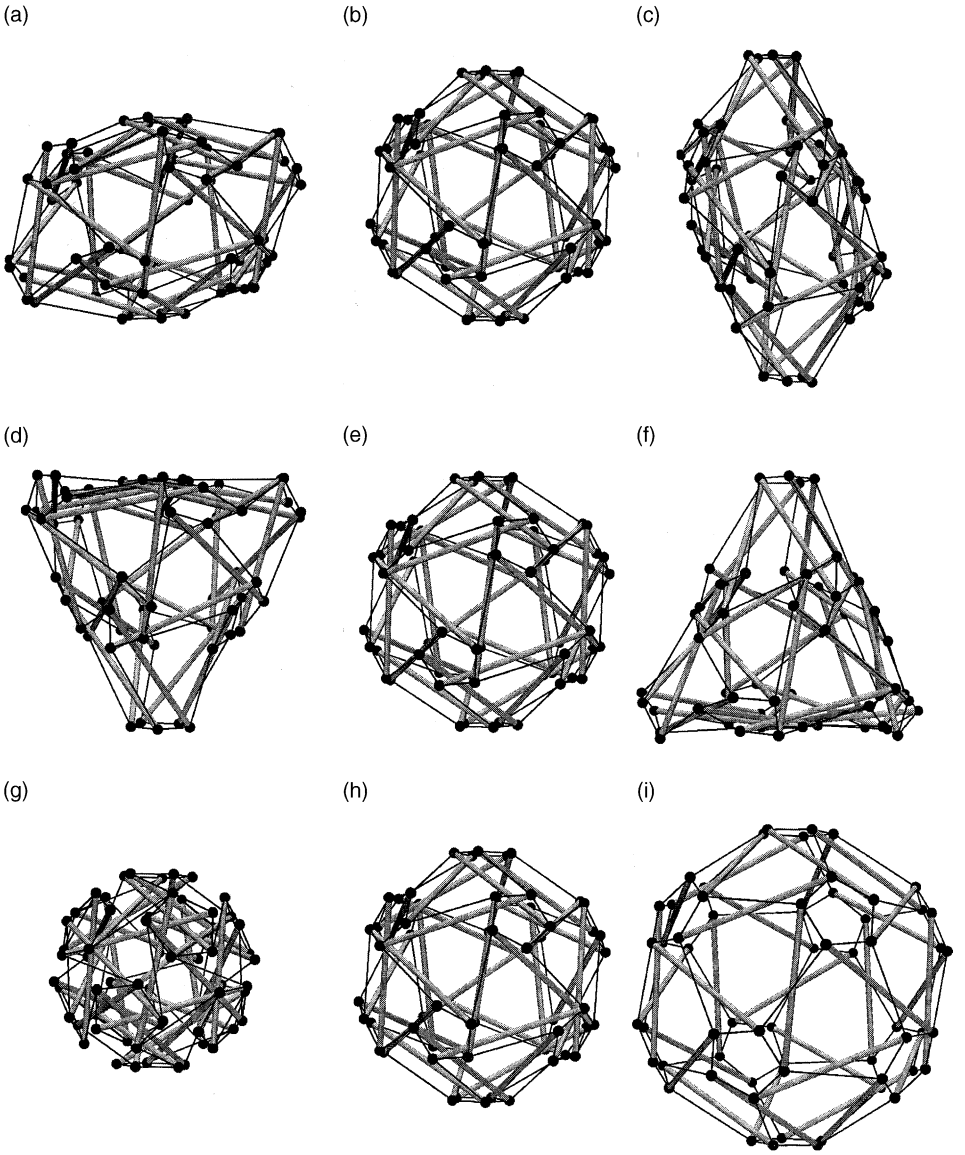

Fig. 6. Mode shapes of a regular truncated icosahedral tensegrity module associated with the first natural frequency (a, b, c), the second natural frequency (d, e, f), and the third natural frequency (g, h, i).

cables in the tensegrity module. If one truncates the dodecahedron by cutting off each vertex along a plane perpendicular to the radius, equilateral triangles are created. The truncating equilateral triangles in the tensegrity module in Fig. 2c are twisted by a specific angle α compared to the equilateral triangles in Fig. 2b. There are 3×20 nodes in both the truncated dodecahedron and the truncated dodecahedral tensegrity module, $n_{\mathrm{N}} = 60$. Since bars connect these nodes, there are 30 bars. There are 30 vertical cables and 3×20 cables along the truncating triangles. As a result, the number of truss elements is $n_{\mathrm{E}} = 30 + 30 + 60 = 120$. The Maxwell number in Eq. (2) becomes $Mx = 120 - (3 \times 60 - 6) = -54$. Calladine's relation (3) shows

that there are 55 infinitesimal mechanisms, i.e., $n_{\mathrm{M}} = 55$. The above values are exactly the same as those shown in Table 1 for the dual icosahedral tensegrity modules.

4.2. Initial shape finding

There are 60 congruent configurations of a regular dodecahedron. They form the icosahedral group (Grossman and Magnus, 1964; Ledermann, 1961). For a truncated dodecahedron and a regular truncated dodecahedral tensegrity module, it is convenient to use rotation $\mathbf{R}'$ with respect the radius through a vertex by angle $2\pi/3$, i.e., $\mathbf{R}'\mathbf{R}'\mathbf{R}' = \mathbf{I}$. The flip $\mathbf{F}$ is defined as before by the π rotation with respect to a median connecting a pair of opposing edges. Among the fifteen medians which comprise five sets of orthogonal triads, a set of orthogonal medians is selected as the body-fixed Cartesian x'-, y'-, and z'-axes, as well as the inertial Cartesian x-, y-, and z-axes, as illustrated in Fig. 7. In the figure, both coordinate frames coincide. However, as $\mathbf{R}'$ and $\mathbf{F}$ are applied the body-fixed frame $\{x', y', z'\}$ rotates with the dodecahedron while the inertial frame $\{x, y, z\}$ remains stationary.

Let the length of the edges of a regular dodecahedron be denoted by b and the length of the truncated edges be denoted by a. The edges of the regular dodecahedron intercept the coordinate axes at $\pm(\sqrt{5}+3)b/4$, as illustrated in Fig. 7. Further, the edge length of the truncating equilateral triangle becomes $(\sqrt{5}+1)a/2$. The rotation $\mathbf{R}'$ with respect to the radius through vertex 1 is described by the axis $\mathbf{u}'$:

$$\mathbf{u}' = \left[\tfrac{\sqrt{5}-1}{2\sqrt{3}},\ 0,\ \tfrac{\sqrt{5}+1}{2\sqrt{3}}\right]^{\mathrm{T}},$$

and the rotation angle $\phi = 2\pi/3$ in the counter clockwise direction with respect to the body-fixed frame $\{x', y', z'\}$. By using the Euler parameters (Haug, 1989):

$$e_0 = \cos\frac{\phi}{2}, \quad e_1 = \frac{\sqrt{5}-1}{2\sqrt{3}}\sin\frac{\phi}{2}, \quad e_2 = 0, \quad e_3 = \frac{\sqrt{5}+1}{2\sqrt{3}}\sin\frac{\phi}{2}, \tag{23}$$

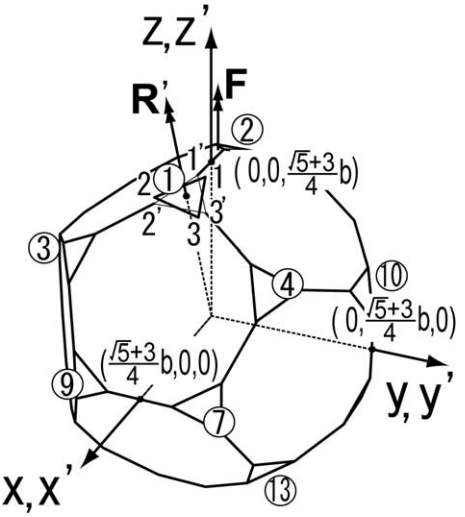

Fig. 7. A body-fixed Cartesian coordinate system $\{x', y', z'\}$ and the inertial Cartesian coordinate system $\{x, y, z\}$ erected for a regular truncated dodecahedron.

the rotation matrix $\mathbf{R}'$ with respect to the body-fixed frame is defined by substituting Eq. (23) into Eq. (9b) with $\phi = 2\pi/3$. The flip $\mathbf{F}$ with respect to the z'-axis by π is defined by the Euler parameters in Eq. (10a) that gives the flip matrix $\mathbf{F}$ in Eq. (10b) with respect to $\{x', y', z'\}$.

Fig. 8a shows a graph of the icosahedral group, redrawn for the generators $\mathbf{R}'$ and $\mathbf{F}$. The solid line $\mathbf{R}'$ in Fig. 8a corresponds to a combination of a solid line and a dashed line, $\mathbf{FR}$, in Fig. 4a. The generators, $\mathbf{R}'$ and $\mathbf{F}$, satisfy the following relations:

$$\mathbf{R}'\mathbf{R}'\mathbf{R}' = \mathbf{I}, \quad \mathbf{F}\mathbf{F} = \mathbf{I}, \quad \mathbf{F}\mathbf{R}'\mathbf{F}\mathbf{R}'\mathbf{F}\mathbf{R}'\mathbf{F}\mathbf{R}'\mathbf{F}\mathbf{R}' = \mathbf{I}. \tag{24}$$

Further, the inverse of $\mathbf{R}'$ and $\mathbf{F}$ are $\mathbf{R}'^{\mathrm{T}}$ and $\mathbf{F}$, respectively.

The graph of the icosahedral group will be used: (i) to generate all nodal coordinates of the tensegrity module starting from the coordinates of node 1 of the twisted truncating triangle 1-2-3 in Fig. 7 and (ii) to define the connections of cable elements.

Let the nodal coordinates be defined at node 1 in Fig. 7. By following the lines in Fig. 8a and performing the $\mathbf{R}'$ or $\mathbf{F}$ operations, one can move node 1 to any desired node identified at the original configuration. The connectivity of tensegrity elements is shown for a positive α in Fig. 8b. In Fig. 8b, the connection of bars is shown by using thick free-hand curves. (For a negative twist angle α the connection of bars become the mirror image of that shown in Fig. 8b with resect to the axis connecting nodes 1 and 4.)

In order to compute nodal coordinates of the tensegrity module with respect to the inertial frame $\{x, y, z\}$, congruent operations with respect to the inertial frame are employed instead of those with respect to the body-fixed frame. The rotation $\mathbf{R}'_{\mathrm{G}}$ describes the rotation with respect to $\mathbf{u}$ by $\phi = 2\pi/3$, where

$$\mathbf{u} = \left[\frac{\sqrt{5}-1}{2\sqrt{3}}, \quad 0, \quad \frac{\sqrt{5}+1}{2\sqrt{3}}\right]^{\mathrm{T}}.$$

The flip with respect to the inertial z-axis is denoted by $\mathbf{F}_{\mathrm{G}}$. The components of $\mathbf{R}'_{\mathrm{G}}$ and $\mathbf{F}_{\mathrm{G}}$ are the same as those of $\mathbf{R}'$ and $\mathbf{F}$.

If $\mathbf{r}_1{}'$ is defined one can obtain $\mathbf{r}_1$ by rotating it with $\mathbf{u}$ by $\phi = -\alpha$ in Eq. (9b):

$$\mathbf{r}_{1'} = b\begin{Bmatrix} \frac{1}{2} - h \\ 0 \\ \frac{3+\sqrt{5}}{4} \end{Bmatrix}, \tag{25a}$$

$$\mathbf{r}_1 = \begin{Bmatrix} \frac{1}{2} - \frac{h}{6}\{3 - \sqrt{5} + (3+\sqrt{5})\cos\alpha\} \\ h\frac{\sqrt{5}+1}{2\sqrt{3}}\sin\alpha \\ \frac{3+\sqrt{5}}{4} - \frac{h}{3}(1-\cos\alpha) \end{Bmatrix}. \tag{25b}$$

By further rotating the coordinates of node 1 with $\mathbf{R}'_{\mathrm{G}}$, nodal coordinates of nodes 2 and 3 can be found. The remaining nodal coordinates are defined in Appendix A.

In order to utilize Eq. (17), the equilibrium equations at node 1 must be constructed. The relevant nodal coordinates are defined as follows:

$$\mathbf{r}_2 = b\begin{Bmatrix} \frac{1}{2} + \frac{h}{12}\{(3+\sqrt{5})(\cos\alpha - \sqrt{3}\sin\alpha) + 2\sqrt{5} - 6\} \\ -\frac{h}{12}(\sqrt{5}+1)(3\cos\alpha + \sqrt{3}\sin\alpha) \\ \frac{3+\sqrt{5}}{4} - \frac{h}{6}(2 + \cos\alpha - \sqrt{3}\sin\alpha) \end{Bmatrix}, \tag{26a}$$

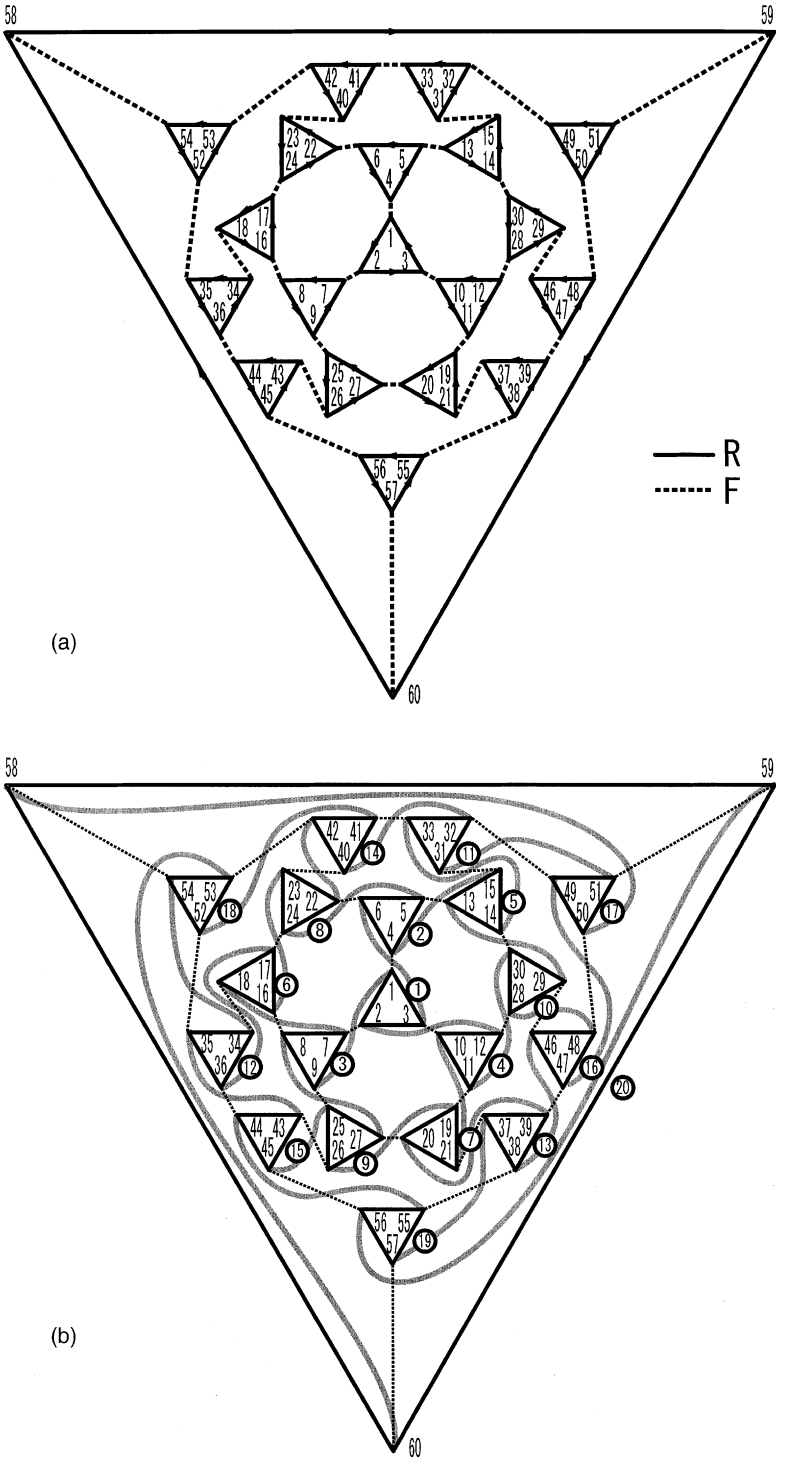

Fig. 8. (a) A graph of the icosahedral group and (b) a connectivity diagram of a truncated dodecahedral tensegrity module with a positive twist angle (thick lines denote bar connections).

$$\mathbf{r}_3 = b\begin{Bmatrix} \frac{1}{2}+\frac{h}{12}\{-6+2\sqrt{5}+(3+\sqrt{5})\cos\alpha+\sqrt{3}(3+\sqrt{5})\sin\alpha\} \\ \frac{h}{12}(\sqrt{5}+1)(3\cos\alpha-\sqrt{3}\sin\alpha) \\ \frac{3+\sqrt{5}}{4}-\frac{h}{6}(2+\cos\alpha+\sqrt{3}\sin\alpha) \end{Bmatrix}, \tag{26b}$$

$$\mathbf{r}_4 = b\begin{Bmatrix} -\frac{1}{2}+\frac{h}{6}\{(3-\sqrt{5})+(3+\sqrt{5})\cos\alpha\} \\ -\frac{h}{2\sqrt{3}}(\sqrt{5}+1)\sin\alpha \\ \frac{3+\sqrt{5}}{4}-\frac{h}{3}(1-\cos\alpha) \end{Bmatrix}, \tag{26c}$$

$$\mathbf{r}_9 = b\begin{Bmatrix} \frac{1+\sqrt{5}}{4}+\frac{h}{6}\{1-\sqrt{5}+(2+\sqrt{5})\cos\alpha-\sqrt{3}\sin\alpha\} \\ -\frac{\sqrt{5}+1}{4}+\frac{h}{12}\{(\sqrt{5}-1)(2+\cos\alpha)-\sqrt{3}(\sqrt{5}+3)\sin\alpha\} \\ \frac{\sqrt{5}+1}{4}-\frac{h}{12}(\sqrt{5}+1)\{3-\sqrt{5}(1-\cos\alpha)+\sqrt{3}\sin\alpha\} \end{Bmatrix}. \tag{26d}$$

The lengths of bars, vertical cables, and truncating edge cables, l_b, l_v, and l_t, become:

$$l_b = \|\mathbf{r}_9-\mathbf{r}_1\|, \quad l_v = \|\mathbf{r}_4-\mathbf{r}_1\|, \quad l_t = \|\mathbf{r}_2-\mathbf{r}_1\|. \tag{27}$$

The equilibrium equations at node 1 becomes

$$(\mathbf{r}_9-\mathbf{r}_1)\frac{s_b}{l_b}+(\mathbf{r}_4-\mathbf{r}_1)\frac{s_v}{l_v}+(\mathbf{r}_2-\mathbf{r}_1+\mathbf{r}_3-\mathbf{r}_1)\frac{s_t}{l_t}=\mathbf{0}. \tag{28}$$

By setting the determinant of the coefficient matrix of Eq. (28) to zero, the characteristic equation for the twist angle α and the truncation ratio h ($\equiv a/b$) is obtained:

$$\begin{aligned} &2h^2\Big[-8\cos^3\alpha-2(7-3\sqrt{5})\cos^2\alpha+\Big\{6\sqrt{5}-8+2\sqrt{3}(3\sqrt{5}-7)\sin\alpha\Big\}\cos\alpha \\ &\quad+\Big\{3(1-\sqrt{5})+2\sqrt{3}(7-3\sqrt{5})\sin\alpha\Big\}\Big]+3h\Big[2(3-\sqrt{5})\Big\{\cos^2\alpha+(2+\sqrt{3}\sin\alpha)\cos\alpha-2\sqrt{3}\sin\alpha\Big\} \\ &\quad+3(1+\sqrt{5})\Big]-18(\cos\alpha-\sqrt{3}\sin\alpha)=0. \end{aligned} \tag{29}$$

The corresponding pre-stress mode becomes

$$\frac{s_v}{l_v} = -\frac{s_b}{l_b}\frac{6+h\{-6+2\sqrt{5}+(3+\sqrt{5})(\cos\alpha+\sqrt{3}\sin\alpha)\}}{6-2h\{3-\sqrt{5}+(3+\sqrt{5})\cos\alpha\}}, \tag{30a}$$

$$\frac{s_t}{l_t} = -\frac{s_b}{l_b}\frac{6+h\{-6+2\sqrt{5}+(9+\sqrt{5})\cos\alpha+\sqrt{3}(1+\sqrt{5})\sin\alpha\}}{12h\cos\alpha}. \tag{30b}$$

Fig. 9a shows the twist angle α as a function of the truncation ratio h. The twist angle α tends to $\pi/6$ ($=30°$) as $h\to 0$ while α tends to zero as $h\to 1/2$. The figure also shows that the maximum value of the cable tension approaches minimum as $h\to 1/2$. (The optimum dodecahedral tensegrity with $h=1/2$ is not possible to build.) The corresponding pre-stress modes are plotted in Fig. 9b for $0<h<1/2$. The pre-stress modes satisfy the tensegrity condition with $s_v>0$ and $s_t>0$ if $s_b<0$ in the range. Further, the maximum value of the cable tension is always less than the absolute value of bar compression.

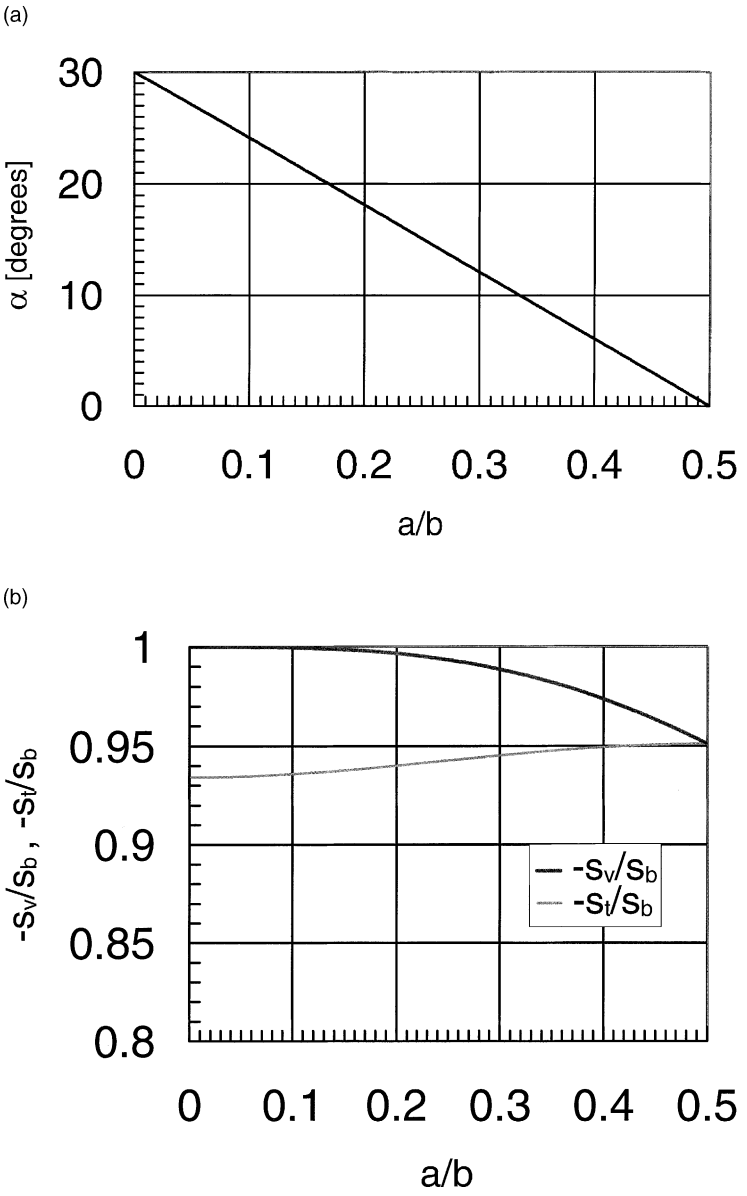

Fig. 9. (a) The twist angle α versus the truncation ratio $h(\equiv a/b)$ for regular truncated dodecahedral tensegrity modules and (b) the pre-stress mode versus the truncation ratio h for regular truncated dodecahedral tensegrity modules.

4.3. Modal analyses of regular truncated dodecahedral tensegrity modules

For a given bar force $s_b < 0$ and the twist angle $\alpha = 15^\circ$, modal analyses as defined in Eqs. (7a)–(7f) were conducted. Similar to regular icosahedral tensegrity modules, there are 15 natural frequencies associated with infinitesimal mechanism modes. Table 3 shows natural frequencies in Hz with increasing pre-stress amplitudes $|s_b|$. The table also shows the number of modes associated with each natural frequency in parentheses. The natural frequencies of infinitesimal mechanism modes, whose stiffness is due to pre-stress,

Table 3
Natural frequencies in Hz and algebraic multiplicities of regular truncated dodecahedral tensegrity modules for increasing pre-stress amplitudes

$\lvert s_b \rvert$	10(N)	50(N)	100(N)	500(N)	1000(N)
1st	1.08(5)	2.41(5)	3.40(5)	7.59(5)	10.71(5)
2nd	1.44(5)	3.23(5)	4.57(5)	10.21(5)	14.43(5)
3rd	1.54(4)	3.45(4)	4.87(4)	10.88(4)	15.35(4)
4th	1.75(3)	3.92(3)	5.55(3)	12.41(3)	17.54(3)
5th	2.50(4)	5.59(4)	7.90(4)	17.67(4)	24.97(4)
6th	2.55(3)	5.70(3)	8.07(3)	18.03(3)	25.50(3)
7th	3.12(1)	7.19(1)	10.17(1)	22.73(1)	32.14(1)
8th	3.85(3)	8.61(3)	12.18(3)	27.23(3)	38.49(3)
9th	4.54(5)	10.16(5)	14.36(5)	32.11(5)	45.40(5)
10th	4.56(3)	10.19(3)	14.41(3)	32.23(3)	45.57(3)
11th	4.61(4)	10.31(4)	14.59(4)	32.62(4)	46.12(4)
12th	4.78(4)	10.69(4)	15.11(4)	33.80(4)	47.79(4)
13th	6.38(3)	14.28(3)	20.19(3)	45.14(3)	63.83(3)
14th	6.46(5)	14.45(5)	20.43(5)	45.67(5)	64.57(5)
15th	7.33(3)	16.39(3)	23.17(3)	51.81(3)	73.27(3)
16th	239.74(3)	240.14(3)	240.63(3)	244.56(3)	249.38(3)
17th	315.06(5)	315.23(5)	315.45(5)	317.17(5)	319.31(5)
18th	363.15(4)	363.29(4)	363.47(4)	364.86(4)	366.59(4)

increase proportionally to the square root of the amplitude of pre-stress, as seen in Eq. (7f). Natural frequencies higher than the 15th correspond to deformation modes and do not change significantly with increasing pre-stress amplitude.

Corresponding to five sets of orthogonal triads formed by medians of a regular dodecahedron, there are five modes associated with the first natural frequency. The first mode deforms to form ellipsoids, as illustrated in Fig. 10a–c. A mode associated with the second natural frequency is shown in Fig. 10d–f. In the second mode, a pair of opposing pentagons is twisting in opposite directions. The third mode is shown in Fig. 10g–i. A diagonal, which vertically connects opposing triangles, translates similar to the modes in Fig. 6d–f. The mode of the seventh frequency corresponds to the spherically symmetric infinitesimal mechanism mode.

5. Conclusions

For regular truncated icosahedral and dodecahedral tensegrity modules, nodal coordinates and connectivity of tensegrity elements were defined by using the graphs of the icosahedral group. A simple method of imposing the existence condition of a pre-stress mode was derived. By using this simplified condition, the initial configurations and the pre-stress modes were analytically obtained. The pre-stress mode shows that cable tension is always less than the absolute value of bar compression. Further, for regular truncated icosahedral tensegrity modules the optimum truncation ratio 0.36 and the corresponding twist angle 18° were found. Finally, by performing modal analyses infinitesimal mechanism modes were classified into subspaces based upon natural frequencies. For both icosahedral and dodecahedral tensegrity modules, the five modes associated with the first natural frequency exhibit ellipsoidal deformation with respect to an orthogonal triad formed by medians. Spherically symmetric modes appear without algebraic multiplicity. These modes correspond to the third natural frequency for regular truncated icosahedral tensegrity modules and the seventh natural frequency for regular truncated dodecahedral tensegrity modules. The natural frequencies of infinitesimal mechanism modes increase proportionally to the square root of the amplitude of pre-stress.

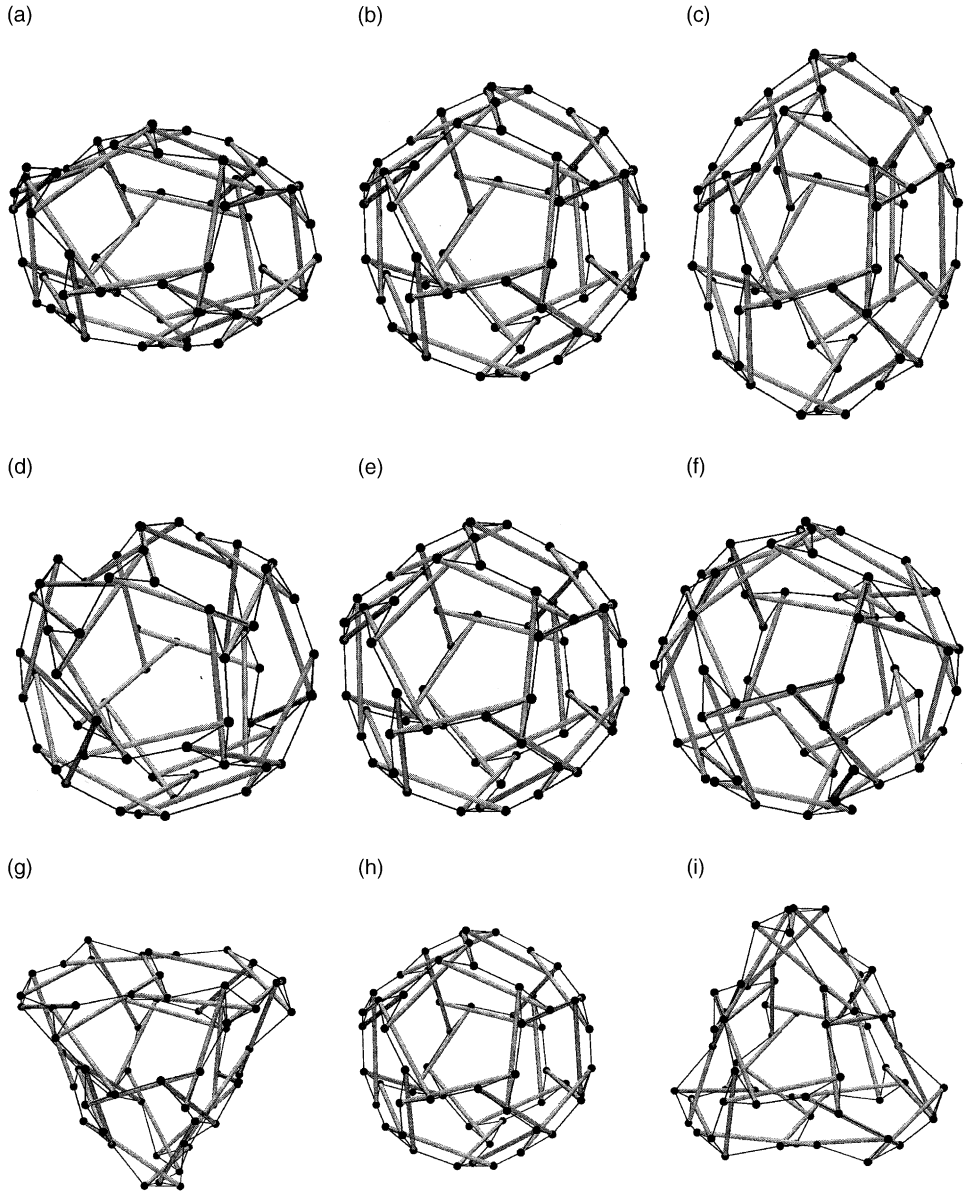

Fig. 10. Mode shapes of a regular truncated dodecahedral tensegrity module associated with the first natural frequency (a, b, c), the second natural frequency (d, e, f), and the third natural frequency (g, h, i).

Acknowledgements

The authors would like to thank Professor Emeritus Theodore Frankel in the Department of Mathematics at University of California, San Diego for his helpful discussions related to algebraic topology and group theory.

Appendix A

Nodal coordinates with respect to the inertial frame $\{x, y, z\}$ of a regular truncated icosahedral tensegrity module are computed by performing the $\mathbf{R}_G$ and $\mathbf{F}_G$ operations on the coordinates of nodes 1–5. The results are

$$\{\mathbf{r}_6,\ \mathbf{r}_7,\ \mathbf{r}_8,\ \mathbf{r}_9,\ \mathbf{r}_{10}\} = \mathbf{F}_G\{\mathbf{r}_1,\ \mathbf{r}_2,\ \mathbf{r}_3,\ \mathbf{r}_4,\ \mathbf{r}_5\}, \tag{A.1}$$

$$\{\mathbf{r}_{11},\ \mathbf{r}_{12},\ \mathbf{r}_{13},\ \mathbf{r}_{14},\ \mathbf{r}_{15}\} = \mathbf{R}_G\mathbf{F}_G\{\mathbf{r}_1,\ \mathbf{r}_2,\ \mathbf{r}_3,\ \mathbf{r}_4,\ \mathbf{r}_5\}, \tag{A.2}$$

$$\{\mathbf{r}_{16},\ \mathbf{r}_{17},\ \mathbf{r}_{18},\ \mathbf{r}_{19},\ \mathbf{r}_{20}\} = \mathbf{R}_G^2\mathbf{F}_G\{\mathbf{r}_1,\ \mathbf{r}_2,\ \mathbf{r}_3,\ \mathbf{r}_4,\ \mathbf{r}_5\}, \tag{A.3}$$

$$\{\mathbf{r}_{21},\ \mathbf{r}_{22},\ \mathbf{r}_{23},\ \mathbf{r}_{24},\ \mathbf{r}_{25}\} = \mathbf{R}_G^3\mathbf{F}_G\{\mathbf{r}_1,\ \mathbf{r}_2,\ \mathbf{r}_3,\ \mathbf{r}_4,\ \mathbf{r}_5\}, \tag{A.4}$$

$$\{\mathbf{r}_{26},\ \mathbf{r}_{27},\ \mathbf{r}_{28},\ \mathbf{r}_{29},\ \mathbf{r}_{30}\} = \mathbf{R}_G^4\mathbf{F}_G\{\mathbf{r}_1,\ \mathbf{r}_2,\ \mathbf{r}_3,\ \mathbf{r}_4,\ \mathbf{r}_5\}, \tag{A.5}$$

$$\{\mathbf{r}_{31},\ \mathbf{r}_{32},\ \mathbf{r}_{33},\ \mathbf{r}_{34},\ \mathbf{r}_{35}\} = \mathbf{F}_G\mathbf{R}_G^3\mathbf{F}_G\{\mathbf{r}_1,\ \mathbf{r}_2,\ \mathbf{r}_3,\ \mathbf{r}_4,\ \mathbf{r}_5\}, \tag{A.6}$$

$$\{\mathbf{r}_{36},\ \mathbf{r}_{37},\ \mathbf{r}_{38},\ \mathbf{r}_{39},\ \mathbf{r}_{40}\} = \mathbf{R}_G\mathbf{F}_G\mathbf{R}_G^3\mathbf{F}_G\{\mathbf{r}_1,\ \mathbf{r}_2,\ \mathbf{r}_3,\ \mathbf{r}_4,\ \mathbf{r}_5\}, \tag{A.7}$$

$$\{\mathbf{r}_{41},\ \mathbf{r}_{42},\ \mathbf{r}_{43},\ \mathbf{r}_{44},\ \mathbf{r}_{45}\} = \mathbf{R}_G^2\mathbf{F}_G\mathbf{R}_G^3\mathbf{F}_G\{\mathbf{r}_1,\ \mathbf{r}_2,\ \mathbf{r}_3,\ \mathbf{r}_4,\ \mathbf{r}_5\}, \tag{A.8}$$

$$\{\mathbf{r}_{46},\ \mathbf{r}_{47},\ \mathbf{r}_{48},\ \mathbf{r}_{49},\ \mathbf{r}_{50}\} = \mathbf{R}_G^3\mathbf{F}_G\mathbf{R}_G^3\mathbf{F}_G\{\mathbf{r}_1,\ \mathbf{r}_2,\ \mathbf{r}_3,\ \mathbf{r}_4,\ \mathbf{r}_5\}, \tag{A.9}$$

$$\{\mathbf{r}_{51},\ \mathbf{r}_{52},\ \mathbf{r}_{53},\ \mathbf{r}_{54},\ \mathbf{r}_{55}\} = \mathbf{R}_G^4\mathbf{F}_G\mathbf{R}_G^3\mathbf{F}_G\{\mathbf{r}_1,\ \mathbf{r}_2,\ \mathbf{r}_3,\ \mathbf{r}_4,\ \mathbf{r}_5\}, \tag{A.10}$$

$$\{\mathbf{r}_{56},\ \mathbf{r}_{57},\ \mathbf{r}_{58},\ \mathbf{r}_{59},\ \mathbf{r}_{60}\} = \mathbf{F}_G\mathbf{R}_G^2\mathbf{F}_G\mathbf{R}_G^3\mathbf{F}_G\{\mathbf{r}_1,\ \mathbf{r}_2,\ \mathbf{r}_3,\ \mathbf{r}_4,\ \mathbf{r}_5\}. \tag{A.11}$$

The nodal coordinates with respect to the inertial frame $\{x, y, z\}$ of a regular truncated dodecahedral tensegrity module are computed by performing the $\mathbf{R}'_G$ and $\mathbf{F}_G$ operations on the coordinates of nodes 1–3. The results are

$$\{\mathbf{r}_4,\ \mathbf{r}_5,\ \mathbf{r}_6\} = \mathbf{F}_G\{\mathbf{r}_1,\ \mathbf{r}_2,\ \mathbf{r}_3\}, \tag{A.12}$$

$$\{\mathbf{r}_7,\ \mathbf{r}_8,\ \mathbf{r}_9\} = \mathbf{R}'_G\mathbf{F}_G\{\mathbf{r}_1,\ \mathbf{r}_2,\ \mathbf{r}_3\}, \tag{A.13}$$

$$\{\mathbf{r}_{10},\ \mathbf{r}_{11},\ \mathbf{r}_{12}\} = \mathbf{R}'^2_G\mathbf{F}_G\{\mathbf{r}_1,\ \mathbf{r}_2,\ \mathbf{r}_3\}, \tag{A.14}$$

$$\{\mathbf{r}_{13},\ \mathbf{r}_{14},\ \mathbf{r}_{15}\} = \mathbf{F}_G\mathbf{R}'_G\mathbf{F}_G\{\mathbf{r}_1,\ \mathbf{r}_2,\ \mathbf{r}_3\}, \tag{A.15}$$

$$\{\mathbf{r}_{16},\ \mathbf{r}_{17},\ \mathbf{r}_{18}\} = \mathbf{R}'_G\mathbf{F}_G\mathbf{R}'_G\mathbf{F}_G\{\mathbf{r}_1,\ \mathbf{r}_2,\ \mathbf{r}_3\}, \tag{A.16}$$

$$\{\mathbf{r}_{19},\ \mathbf{r}_{20},\ \mathbf{r}_{21}\} = \mathbf{R}'^2_G\mathbf{F}_G\mathbf{R}'_G\mathbf{F}_G\{\mathbf{r}_1,\ \mathbf{r}_2,\ \mathbf{r}_3\}, \tag{A.17}$$

$$\{\mathbf{r}_{22},\ \mathbf{r}_{23},\ \mathbf{r}_{24}\} = \mathbf{F}_G\mathbf{R}'^2_G\mathbf{F}_G\{\mathbf{r}_1,\ \mathbf{r}_2,\ \mathbf{r}_3\}, \tag{A.18}$$

$$\{\mathbf{r}_{25},\ \mathbf{r}_{26},\ \mathbf{r}_{27}\} = \mathbf{R}'_G\mathbf{F}_G\mathbf{R}'^2_G\mathbf{F}_G\{\mathbf{r}_1,\ \mathbf{r}_2,\ \mathbf{r}_3\}, \tag{A.19}$$

$$\{\mathbf{r}_{28},\ \mathbf{r}_{29},\ \mathbf{r}_{30}\} = \mathbf{R}'^2_G\mathbf{F}_G\mathbf{R}'^2_G\mathbf{F}_G\{\mathbf{r}_1,\ \mathbf{r}_2,\ \mathbf{r}_3\}, \tag{A.20}$$

$$\{\mathbf{r}_{31},\ \mathbf{r}_{32},\ \mathbf{r}_{33}\} = \mathbf{F}_G\mathbf{R}'_G\mathbf{F}_G\mathbf{R}'^2_G\mathbf{F}_G\{\mathbf{r}_1,\ \mathbf{r}_2,\ \mathbf{r}_3\}, \tag{A.21}$$

$$\{\mathbf{r}_{34},\ \mathbf{r}_{35},\ \mathbf{r}_{36}\} = \mathbf{R}'_{\mathrm{G}}\mathbf{F}_{\mathrm{G}}\mathbf{R}'_{\mathrm{G}}\mathbf{F}_{\mathrm{G}}\mathbf{R}'^{2}_{\mathrm{G}}\mathbf{F}_{\mathrm{G}}\{\mathbf{r}_1,\ \mathbf{r}_2,\ \mathbf{r}_3\}, \tag{A.22}$$

$$\{\mathbf{r}_{37},\ \mathbf{r}_{38},\ \mathbf{r}_{39}\} = \mathbf{R}'^{2}_{\mathrm{G}}\mathbf{F}_{\mathrm{G}}\mathbf{R}'_{\mathrm{G}}\mathbf{F}_{\mathrm{G}}\mathbf{R}'^{2}_{\mathrm{G}}\mathbf{F}_{\mathrm{G}}\{\mathbf{r}_1,\ \mathbf{r}_2,\ \mathbf{r}_3\}, \tag{A.23}$$

$$\{\mathbf{r}_{40},\ \mathbf{r}_{41},\ \mathbf{r}_{42}\} = \mathbf{F}_{\mathrm{G}}\mathbf{R}'^{2}_{\mathrm{G}}\mathbf{F}_{\mathrm{G}}\mathbf{R}'_{\mathrm{G}}\mathbf{F}_{\mathrm{G}}\{\mathbf{r}_1,\ \mathbf{r}_2,\ \mathbf{r}_3\}, \tag{A.24}$$

$$\{\mathbf{r}_{43},\ \mathbf{r}_{44},\ \mathbf{r}_{45}\} = \mathbf{R}'_{\mathrm{G}}\mathbf{F}_{\mathrm{G}}\mathbf{R}'^{2}_{\mathrm{G}}\mathbf{F}_{\mathrm{G}}\mathbf{R}'_{\mathrm{G}}\mathbf{F}_{\mathrm{G}}\{\mathbf{r}_1,\ \mathbf{r}_2,\ \mathbf{r}_3\}, \tag{A.25}$$

$$\{\mathbf{r}_{46},\ \mathbf{r}_{47},\ \mathbf{r}_{48}\} = \mathbf{R}'^{2}_{\mathrm{G}}\mathbf{F}_{\mathrm{G}}\mathbf{R}'^{2}_{\mathrm{G}}\mathbf{F}_{\mathrm{G}}\mathbf{R}'_{\mathrm{G}}\mathbf{F}_{\mathrm{G}}\{\mathbf{r}_1,\ \mathbf{r}_2,\ \mathbf{r}_3\}, \tag{A.26}$$

$$\{\mathbf{r}_{49},\ \mathbf{r}_{50},\ \mathbf{r}_{51}\} = \mathbf{F}_{\mathrm{G}}\mathbf{R}'_{\mathrm{G}}\mathbf{F}_{\mathrm{G}}\mathbf{R}'^{2}_{\mathrm{G}}\mathbf{F}_{\mathrm{G}}\mathbf{R}'_{\mathrm{G}}\mathbf{F}_{\mathrm{G}}\{\mathbf{r}_1,\ \mathbf{r}_2,\ \mathbf{r}_3\}, \tag{A.27}$$

$$\{\mathbf{r}_{52},\ \mathbf{r}_{53},\ \mathbf{r}_{54}\} = \mathbf{R}'_{\mathrm{G}}\mathbf{F}_{\mathrm{G}}\mathbf{R}'_{\mathrm{G}}\mathbf{F}_{\mathrm{G}}\mathbf{R}'^{2}_{\mathrm{G}}\mathbf{F}_{\mathrm{G}}\mathbf{R}'_{\mathrm{G}}\mathbf{F}_{\mathrm{G}}\{\mathbf{r}_1,\ \mathbf{r}_2,\ \mathbf{r}_3\}, \tag{A.28}$$

$$\{\mathbf{r}_{55},\ \mathbf{r}_{56},\ \mathbf{r}_{57}\} = \mathbf{R}'^{2}_{\mathrm{G}}\mathbf{F}_{\mathrm{G}}\mathbf{R}'_{\mathrm{G}}\mathbf{F}_{\mathrm{G}}\mathbf{R}'^{2}_{\mathrm{G}}\mathbf{F}_{\mathrm{G}}\mathbf{R}'_{\mathrm{G}}\mathbf{F}_{\mathrm{G}}\{\mathbf{r}_1,\ \mathbf{r}_2,\ \mathbf{r}_3\}, \tag{A.29}$$

$$\{\mathbf{r}_{58},\ \mathbf{r}_{59},\ \mathbf{r}_{60}\} = \mathbf{F}_{\mathrm{G}}\mathbf{R}'^{2}_{\mathrm{G}}\mathbf{F}_{\mathrm{G}}\mathbf{R}'_{\mathrm{G}}\mathbf{F}_{\mathrm{G}}\mathbf{R}'^{2}_{\mathrm{G}}\mathbf{F}_{\mathrm{G}}\mathbf{R}'_{\mathrm{G}}\mathbf{F}_{\mathrm{G}}\{\mathbf{r}_1,\ \mathbf{r}_2,\ \mathbf{r}_3\}. \tag{A.30}$$

References

Argyris, J.H., Scharpf, D.W., 1972. Large deflection analysis of prestressed networks. ASCE Journal of the Structural Division 98 (ST3), 633–654.

Calladine, C.R., 1978. Buckminster Fuller's tensegrity structures and Clerk Maxwell's rules for the construction of stiff frames. International Journal of Solids and Structures 14, 161–172.

Chung, F., Sternberg, S., 1993. Mathematics and the buckyball. American Scientist 81 (January–February), 56–71.

Curl, R.E., Smalley, R.E., 1988. Probing C_{60}. Science 242 (November), 1017–1022.

Frankel, T., 1997. The Geometry of Physics. Cambridge, New York.

Grossman, I., Magnus, W., 1964. Groups and Their Graphs. The Mathematical Association of America, Washington.

Haug, E.J., 1989. Computer Aided Kinematics and Dynamics of Mechanical Systems, vol. 1: Basic Methods. Allyn and Bacon, Boston.

Kenner, H., 1976. Geodesic Math and How to Use It. University of California Press, Berkeley, CA.

Kroto, H., 1988. Space, stars, C_{60}, and soot. Science 242 (November), 1139–1145.

Ingber, D.E., 1998. The architecture of life. Scientific American, January issue, pp. 2–11.

Ledermann, W., 1961. Introduction to the Theory of Finite Groups. Oliver and Boyd, New York.

Marks, R., Fuller, B.R., 1973. The Dymaxion World of Buckminster Fuller. Anchor Books, Garden City, NY.

Maxwell, J.C., 1864. On the calculation of the equilibrium and stiffness of frames. Philosophical Magazine 27, 250.

Maxwell, J.C., 1890. In: W.D. Niven (Ed.), The Scientific Papers of James Clark Maxwell. Dover, New York, pp. 598–604.

Murakami, H., 2001a. Static and dynamic analysis of tensegrity structures. Part 1. Nonlinear equations of motion. International Journal of Solids and Structures 38 (20), 3599–3613.

Murakami, H., 2001b. Static and dynamic analysis of tensegrity structures. Part 2. Quasi-static analyses. International Journal of Solids and Structures 38 (20), 3615–3629.

Murakami, H., Nishimura, Y., 1999. Static and dynamic characterization of tensegrity modules. Proceedings of ASME DETC99, Las Vegas, 12–15 September, 1999, p. 9.

Murakami, H., Nishimura, Y., 2000. Static and dynamic characterization of some tensegrity modules. ASME Journal of Applied Mechanics 67 (4).

Pellegrino, S., Calladine, C.R., 1986. Matrix analysis of statically and kinematically indeterminate frameworks. International Journal of Solids and Structures 22 (4), 409–428.

Pugh, A., 1976. An Introduction to Tensegrity. University of California Press, Berkeley, CA.

Skelton, R.E., Sultan, C., 1997. Controllable tensegrity, a new class of smart structures. SPIE, San Diego, p. 12.

Sokolnikoff, I.S., 1956. Mathematical Theory of Elasticity. Second ed., McGraw-Hill, New York, Section 26.

Sternberg, S., 1993. Group Theory in Physics. Cambridge University Press, New York.

Sultan, C., 1999. Modeling, Design and Control of Tensegrity Structures with Applications. Ph.D. Dissertation, Purdue University, West Lafayette, IN.